Engineering Failure Analysis xxx (xxxx) 106048

Contents lists available at ScienceDirect

Engineering Failure Analysis

journal homepage: www.elsevier.com/locate/engfailanal

A brief note on monotonic and fatigue fracture events investigation of thin-walled tubular austenitic steel specimens via fracture surface topography analysis (FRASTA)

Wojciech Macek [a], Dhinakaran Sampath [b], Łukasz Pejkowski [c], Krzysztof Żak [d]

[a] Gdańsk University of Technology, Faculty of Mechanical Engineering and Ship Technology, Gabriela Narutowicza11/12, 80-233 Gdańsk, Poland
[b] Tata Steel Europe R&D, Swansea SA2 8PP, United Kingdom
[c] Bydgoszcz University of Science and Technology, Faculty of Mechanical Engineering, Kaliskiego 7, 85-796 Bydgoszcz, Poland
[d] Opole University of Technology, Faculty of Mechanical Engineering, Mikołajczyka 5, 45-271 Opole, Poland

ARTICLE INFO

Keywords:
Fractography
Fracture surface analysis
FRASTA
Austenitic stainless steel

ABSTRACT

The main objective of this short communication is to show the fracture progression in each loading case and complement knowledge about fracture mechanisms underpinning the tensile and fatigue performance of thin-walled tubes. For this purpose, the fracture surface topography analysis (FRASTA) method was used in the thin-walled tubular austenitic stainless-steel specimens. Two cases were analyzed: monotonic tension, and uniaxial fully-reversed fatigue. Furthermore, the fractures topographies were quantified through the profiles over their entire surfaces with the support of an optical confocal measurement system. The results showed the usefulness of the FRASTA method in identifying characteristic zones in the cracking process for the analyzed cases and motivates its development for other materials and complex loading cases.

Nomenclature

Δ	Range of a given quantity -
ε	Normal (axial) strain %
λc	Gaussian cut-off filter length, wavelength to determine the bound between surface roughness component and waviness component mm
λs	Gaussian cut-off filter length, wavelength to determine the bound between surface roughness component and other shorter components μm
σ_{y02}	Offset yield stress MPa
σ_u	Ultimate tensile strength MPa
ϵ_{σ_u}	Total strain at maximum stress -
ν_e	elastic Poisson ratio -
d	displacement μm
E	Young modulus GPa

E-mail address: wojciech.macek@pg.edu.pl (W. Macek).

https://doi.org/10.1016/j.engfailanal.2022.106048
Received 4 December 2021; Received in revised form 11 January 2022; Accepted 12 January 2022
1350-6307/

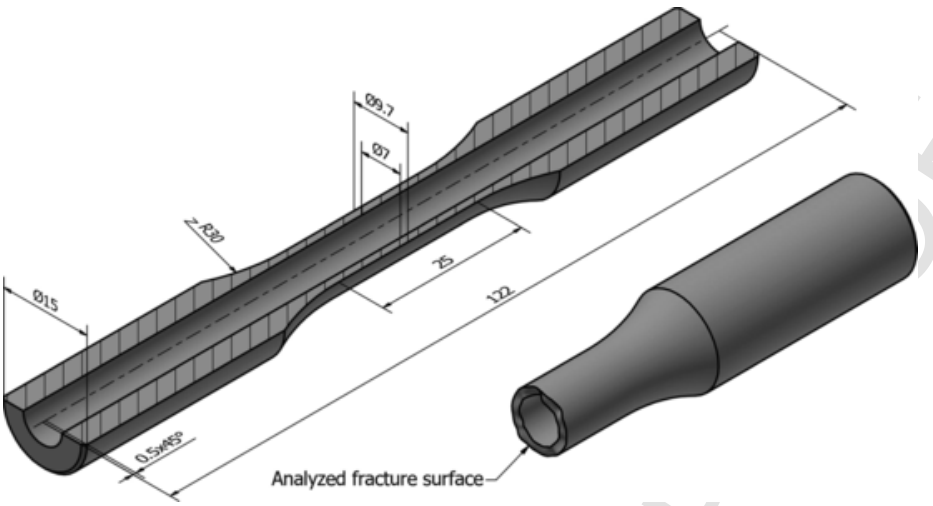

Fig. 1. Specimen shape and geometry.

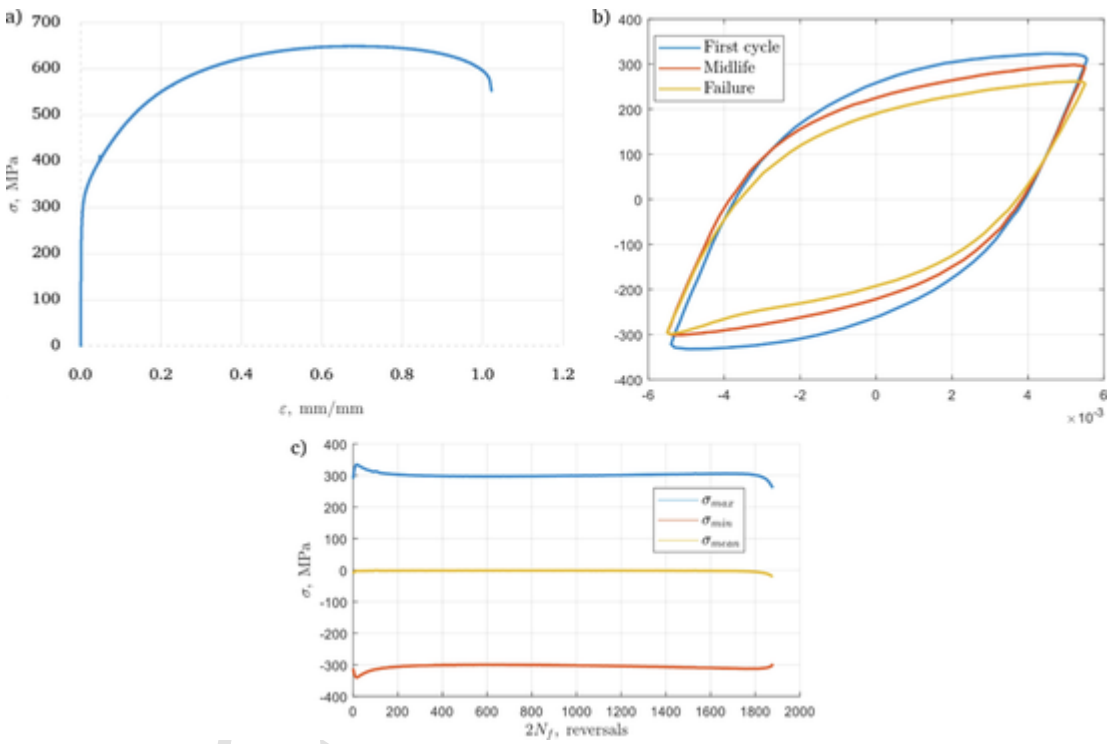

Fig. 2. (a) Monotonic tension stress-strain curve, (b) strain hysteresis loops for a specimen subjected to fatigue test, (c) stress response history.

Nf	Number of cycles to failure cycle
Rp	Maximum peak height of the roughness profile μm
Rv	Maximum valley depth of the roughness profile μm
Rz	Maximum height of roughness profile μm
Rc	Mean height of the roughness profile elements μm
Ra	Arithmetic mean deviation of the roughness profile μm
Rq	Root-mean-square (RMS) deviation of the roughness profileμm
Rdc	Roughness profile section height difference μm

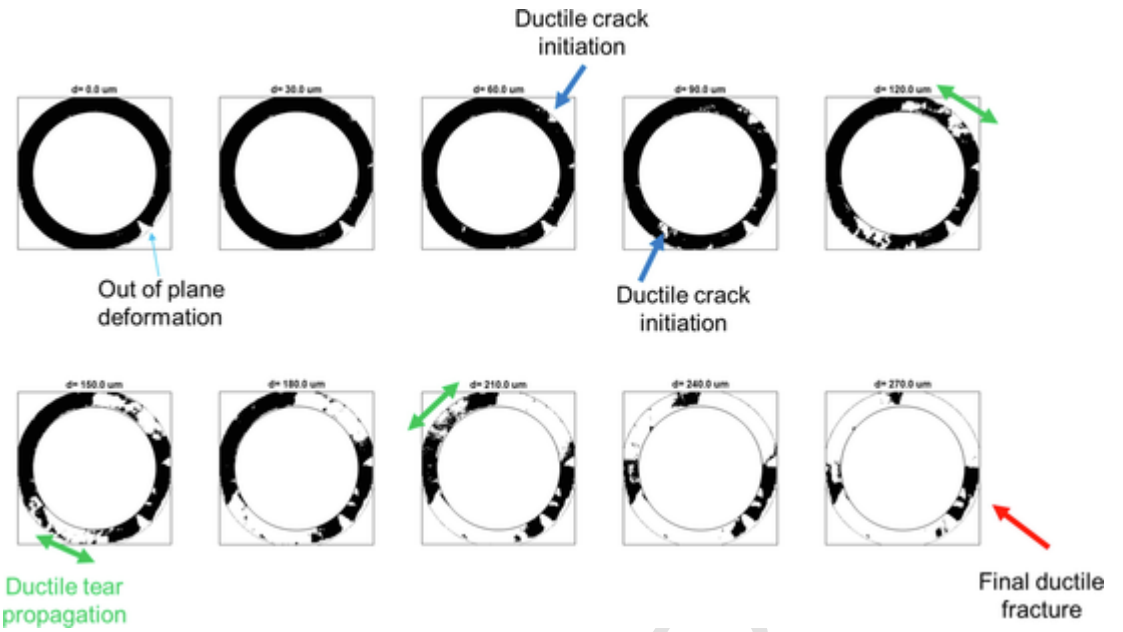

Fig. 3. FAPPs displaying the fracture progression of the thin-walled stainless steel tensile specimen.

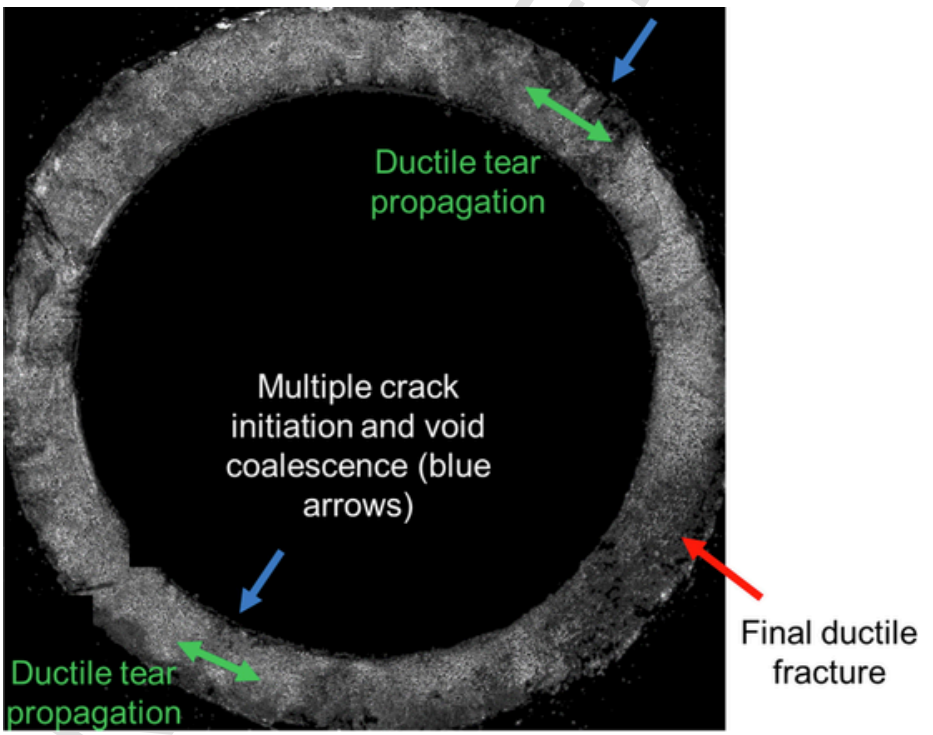

Fig. 4. Crack initiation and propagation regions identified on the monotonic tensile fracture surface using the fracture events revealed by FAPPs.

1. Introduction

An understanding of the axial-torsion fatigue behavior of materials is important in the design of complex engineering components. A thin-walled tubular specimen is used in evaluating the axial-torsion fatigue behavior experimentally [1,2]. Most often, the load–displacement response of the thin-walled specimen to the complex load sequence is used to determine the damage parameters [3–5]. However, the fracture surface information is not widely employed in such analyses despite demonstrating a potential to reveal the correlation between the material structure and mechanical behavior. Extracting fracture surface gives vital information about the

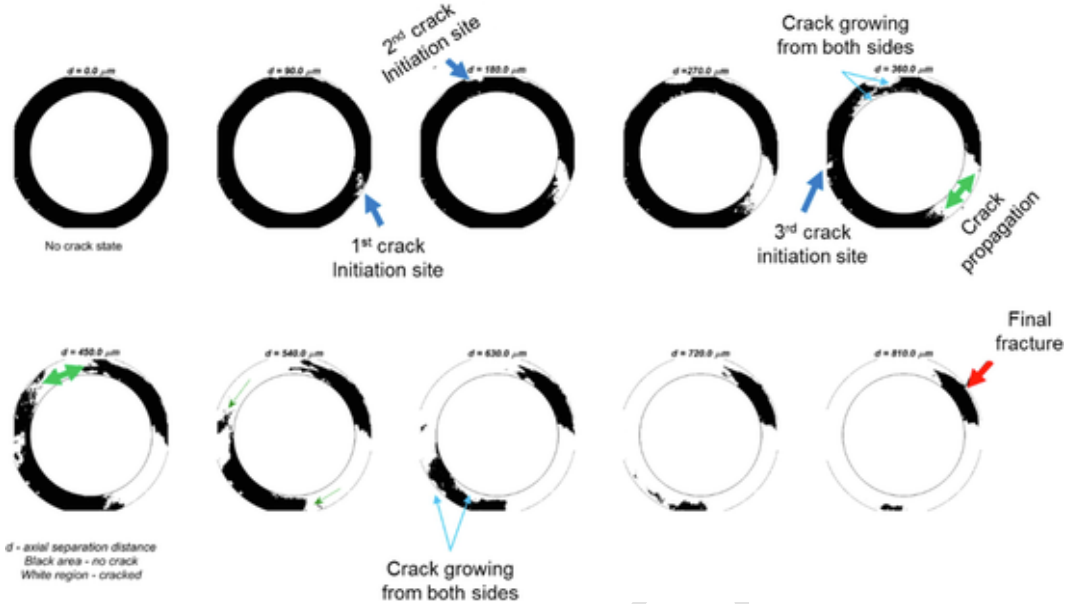

Fig. 5. FAPPs displaying the fracture progression of the thin-walled stainless steel fatigue specimen.

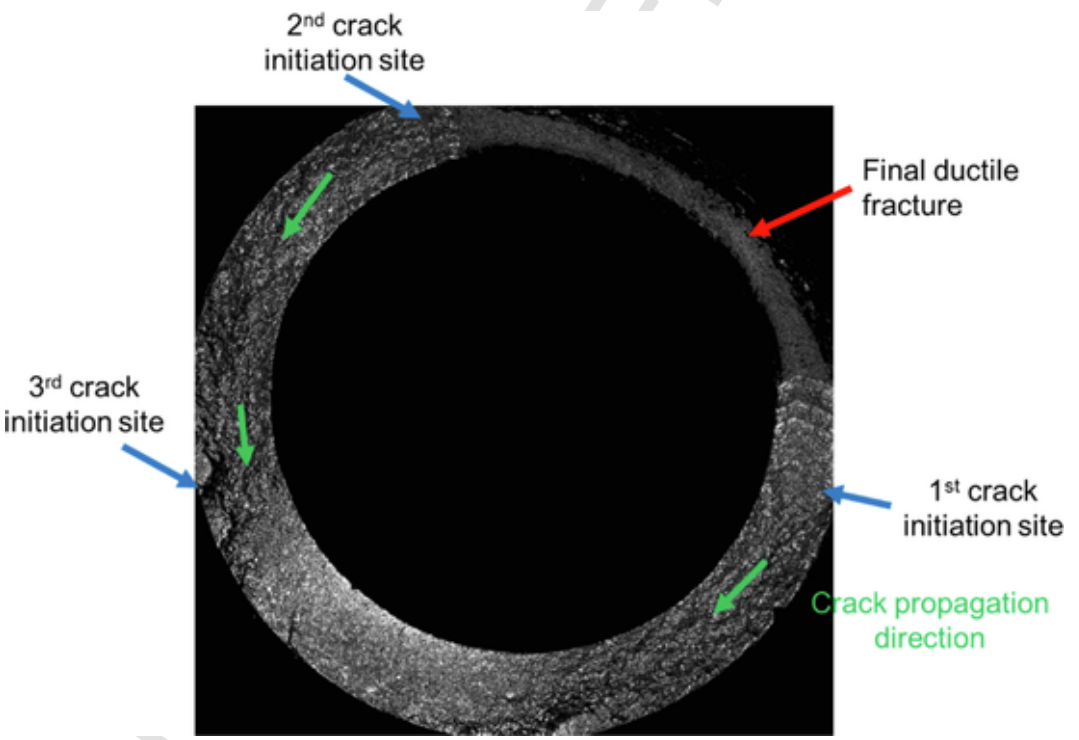

Fig. 6. Crack initiation and propagation regions identified on the fatigue fracture surface using the fracture events revealed by FAPPs.

failure process using post-failure analyses such as qualitative (microscopic examination of fracture surfaces) and quantitative (relation between surface topography parameters and fracture mode, and fracture reconstruction) methods. This kind of analyses was carried out by Macek et al. [6–8], where the relationships between bending-to-torsion ratio or strain sequence to surface topography parameters were demonstrated. This short communication presents the results of a fracture reconstruction method called FRActure Surface Topography Analysis (FRASTA) [9–11] to elucidate the fracture events in thin-walled tubular stainless steel specimens failed under monotonic tensile and fatigue loads. This method has not been applied for thin-walled tubular specimens so far, and it will be ap-

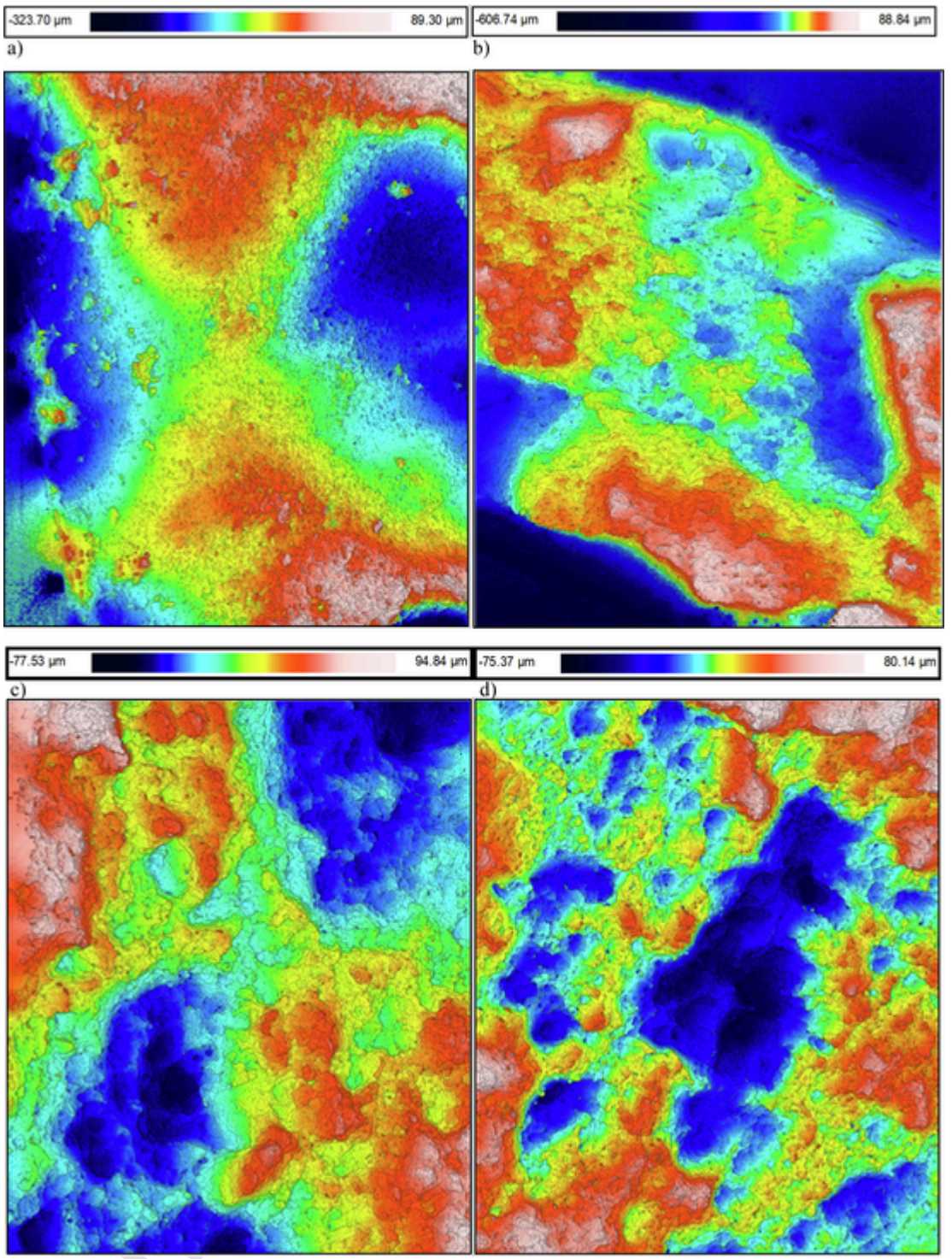

Fig. 7. Characteristic zones of areas of 844.5 × 706.5 µm^2, for monotonic specimen: (a) multiple crack initiation; and for fatigue case: (b) first crack initiation, (c) second crack initiation, (d) final ductile fracture.

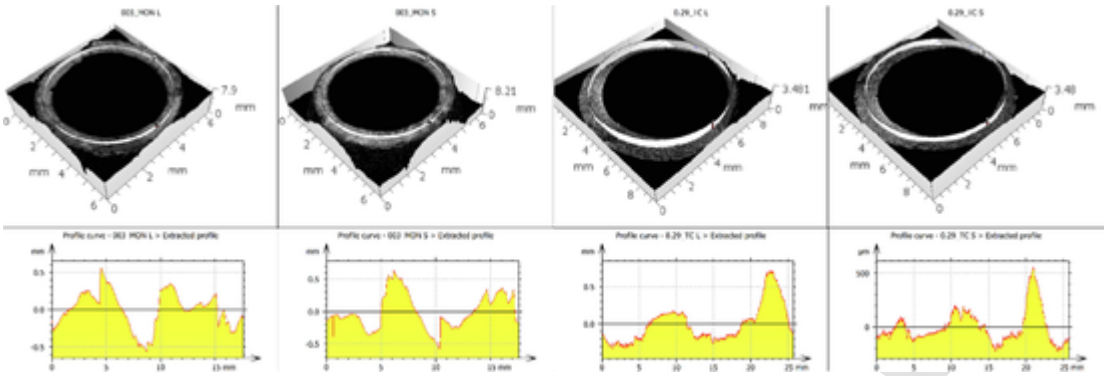

Fig. 8. Original profile for both sides of each specimens.

plied to the axial-torsion fatigue load case later. The identification of critical fracture sites and events will serve not only for the in-depth understanding of fracture mechanisms, but also for the development of fatigue life estimation models [12,13].

2. Methodology

2.1. Monotonic and fatigue test

The experiments were conducted as a part of the previous research by Pejkowski et al. [14,15]. Experimental campaign was aimed to study various aspects of the materials behavior under multiaxial loadings, especially asynchronous cases. The present study considers the part related to the monotonic tension and uniaxial, fully reversed fatigue test only.

Tests were performed on thin-walled, cylindrical specimens (see Fig. 1), manufactured from X5CrNi18-10 austenitic stainless steel. This grade is equivalent to 304/304L steel. All the experiments were conducted on Instron 8874 axial–torsional testing system, equipped with axial and biaxial extensometers to record and control the strain. The basic mechanical properties obtained in tests are [15]: Young modulus $E = 200.8$ GPa, offset yield stress $\sigma_{y02} = 265$ MPa, ultimate tensile strength $\sigma_u = 645.4$ MPa, total strain at maximum stress $\varepsilon_{\sigma_u} = 0.685$, and elastic Poisson ratio $\nu_e = 0.29$. In the fatigue load case being analyzed in the present study, an axial strain amplitude $\Delta\varepsilon/2$ of 0.0055 was applied. The stable stress amplitude, $\Delta\sigma/2$, was 301.1 MPa at midlife, and the fatigue life, $2N_f$, was 3758 reversals.

2.2. Fracture surface topography measurement

After mechanical and fatigue tests, the obtained fractures were subjected to surface measurements. Sensofar S neox optical 3D profiling microscopes were applied for measurements of the surface topography. The Focus variation method was used to measure the topography of fatigue fractures, in the area of 9.09 × 9.36 mm^2 (3250 × 3391 pixels), with a pixel size of 2.76 μm/pixel. The lens used for the measurements is a Nikon EPI 5x. Additional measurements of the characteristic zones (see Fig. 7) were made using the confocal technique with 20× magnification, in the areas of 844.5 × 706.5 μm^2 (1224 × 1024 pixels), with a pixel size of 0.69 μm/pixel. The surface topography parameters and the 3D visualisation of the treated fractures were determined using the Digital Surf MountainsMap software.

2.3. FRASTA

FRActure Surface Topography Analysis (FRASTA) is a quantitative fractographic analysis to reconstruct the fracture events using the complementary fracture surfaces of a failed specimen or a mechanical component. Monotonic and fatigue fractures are complex in terms of the crack initiation and propagation events in a hollow cylindrical stainless steel specimen. In order to understand the fracture progression in the tensile monotonic test and the fatigue test, FRASTA was used to interrogate the fracture surfaces. The analysis involves a simulation of fracture progression from a series of fracture area projection plots (FAPPs) at discretely increasing values of separation distance between the complementary fracture surfaces. A FAPP represents a snapshot of the fracture progression at a given separation distance in which the black and white areas correspond to “no separation” and “separated or cracked” states, respectively. The analysis procedure is described elsewhere [9,10].

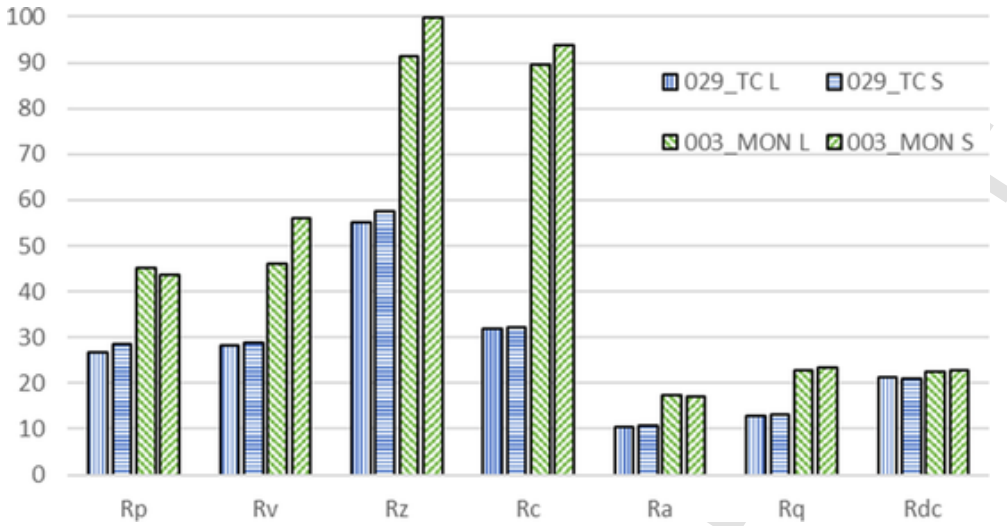

Fig. 9. Filtered parameters results for both sides of each specimens.

3. Results and discussion

3.1. Monotonic and fatigue results

Fig. 2 presents monotonic stress–strain curve, and stress–strain response of a specimen under the fatigue loading. Monotonic tension showed that the material exhibits significant ductility and strain hardening. After initial, very fast hardening and subsequent softening, the stress response was quite stable during the fatigue test at a strain amplitude level$\Delta\varepsilon/2 = 0.0055$.

3.2. FRASTA

Fig. 3 shows a series of FAPPs obtained from the fracture surfaces of the tensile specimen. The initial FAPP at d = 0 was the least separation distance at which there is no distinct crack. Note that the specimen experienced a significant plastic deformation before the crack initiation. The "white" area at the 4o'clock position was due to out-of-plane deformation during the final fracture. Therefore, it was not considered as a crack initiation. The plots demonstrated three stages of fracture progression – crack initiation, ductile tear propagation, and final fracture. The cracks initiated at multiple locations at d ~ 60 and 90 μm, and they initiated on both inner and outer surfaces. This was followed by the ductile tear propagation at d ~ 120 μm from the crack initiation sites into the specimen's cross-section. Thinning of the cross-section section was significant after d = 210 μm due to necking, and following which, the final fracture occurred at d ~ 270 μm. The ductile tear propagation area marked in the FAPP at d = 210 μm shows a mix of "black" and "white" spots with discontinuous crack fronts representing dimples. This feature is also observed at other locations, and it suggests that the crack propagation has occurred by the void coalescence mechanism. The displacement taken for separation is ~ 0.27 mm, which is only a tiny fraction compared with the total displacement taken for fracture (see Fig. 2a). This implies that the crack initiation events would have started after the maximum load and closer to the strain (ε) 0.8–1. The crack initiation and propagation regions are marked on the confocal image of the fracture surface as in Fig. 3 using the fracture events revealed by FAPPs (see Fig. 4).

Fig. 5 shows a series of FAPPs obtained from the fracture surfaces of the fatigue specimen. The FAPP at d = 0 μm was the initial state at which there was no crack. Multiple fatigue crack initiation sites were observed – first site was at d ~ 90 μm and the second site was at d ~ 180 μm. This observation is confirmed by the confocal image of the fatigue specimen (see Fig. 6) with the presence of fatigue beach marks at the first and the second crack initiation sites. The fatigue crack propagation occurred between 180 and 810 μm, and the direction of propagation is marked in Fig. 6. At d ~ 360 μm, the crack initiation occurred at a third site. All the crack fronts propagation around the circumference of the specimen leading to instability at the final fracture region at d ~ 810 μm. This final fracture feature is in agreement with the respective fracture surface image (see Fig. 7) showing excessive plastic deformation before separation compared to the surface created by the fatigue load. The total separation displacement (d) for the fatigue specimen (810 μm) is greater than that for the tensile specimen (270 μm) and this is because the general displacement of the tensile specimen without cracking is excluded. Moreover, the total "d" induced in the fatigue specimen is typical for a $\Delta\varepsilon/2$ of 0.55%. The detailed surface topography of crack initiation, propagation, final fracture regions is shown in Fig. 8. The feasibility of FRASTA method to reveal the fracture events and sites in thin-walled specimens failed by monotonic tensile and fatigue loads is promising. We could therefore extend this method to thin-walled specimens failed by axial-torsion fatigue load.

The areas identified with the FRASTA method are more precisely presented in Fig. 7.

Observing the magnification of the regions identified on the fatigue fracture (see Fig. 7), one can observe the characteristic multi-crack of the material, which may be caused by the structure of the material and voids in its structure. Another reason for this method of cracking may be the very structure of the material and its physical properties.

3.3. Comparing both sides of fracture surfaces and selection of surface profile parameter

Due to the thin-walled nature of the specimens, a circular profile extraction was used (see Fig. 8). The extracted circle had a radius of 4.1 mm, generating profiles 25.76 mm long, with 18,667 points. Additionally, for comparison, a specimen subjected to monotonic loading was tested, for which the extracted circle radius was 2.8 mm. The clockwise direction was applied for the circular extraction.

The profile path were selected at the center of the fracture surface because crack propagation is more stabilized there and moreover it is easier to capture the middle part of the thin-walled tubular surface during measurement which may be slightly deformed, therefore, the center axis is more representative. It also avoids reaching non-measured points that may occur near the edges.

The ISO 4287 standard list the information connect the maximum spacing of data and the value of the micro-roughness cut-off λs to be used. The λs (Gaussian) filter applied on the level 2.5 μm removes scales smaller than the nesting index value of the filter. The λc filter (Gaussian) with a value of 0.8 mm that separates waviness from roughness also is applied. Evaluation length for all λc was 32.

A curious issue that requires clarification is the reciprocity of the measured values of the profiles for both fracture sides. Fig. 9 plots selected values of profile roughness parameters for the long (L) side against those for the short (S) side.

The roughness parameters of the fracture profiles assume clearly higher values for the monotonic specimen than for the fatigued one. The greatest difference occurs for the mean height of the roughness profile elements Rc and amounts to 286%. And the smallest (7.3%) for roughness profile section height difference Rdc parameter.

As for the differences in individual parameters for both sides of the specimens, their averaged values are close to zero. The biggest difference was noted for the Rv parameter (approx. 14%), which shows that any part of the broken elements can be taken into account for the analysis of the surface topography.

4. Conclusions

The difference in the two different cracking mechanisms, monotonic and fatigue, has been studied through FRASTA to evaluate characteristic crack zones. A quantitative analysis of the parameters of the profiles of the tested specimens was also performed for both fractures of each loading case. From this study, the following conclusions are drawn:

- the method turned out to be useful for thin-walled specimens;
- using FRASTA, the areas of crack initiation and the directions of their propagation were identified;
- the FRASTA method applied to thin-walled specimens can be employed for other fatigue loading cases.

In general, profile Rx parameters have been sensitive to the degree of damage case and can be used for quantitative identification of fracture mechanisms.

The roughness profile section height difference (rdc) and the maximum valley depth of the roughness profile (Rv) have exhibited the lowest (0.1%) and highest (14%) differences, respectively, confirming that any side of the specimen's fractures can be analyzed.

For the first time, the FRASTA method has been used to reveal fracture initiation sites and fracture propagation direction in thin-walled tubular specimens under tensile and fatigue loads. This information has provided key insights into the failure mechanisms.

Declaration of Competing Interest

The authors declare that they have no known competing financial interests or personal relationships that could have appeared to influence the work reported in this paper.

References

[1] P. Peralta, C. Laird, Fatigue of Metals, Fifth Edit, Elsevier, Amsterdam, 2014. https://doi.org/10.1016/B978-0-444-53770-6.00018-6.
[2] C.D.S. Souto, V.M.G. Gomes, M. Figueiredo, J.A.F.O. Correia, G. Lesiuk, A.A. Fernandes, A.M.P. De Jesus, Fatigue behaviour of thin-walled cold roll-formed steel sections, Int. J. Fatigue. 149 (2021) 106299, https://doi.org/10.1016/j.ijfatigue.2021.106299.
[3] H. Xin, J.A.F.O. Correia, M. Veljkovic, Y. Zhang, F. Berto, A.M.P. de Jesus, Probabilistic strain-fatigue life performance based on stochastic analysis of structural and WAAM-stainless steels, Eng. Fail. Anal. 127 (2021) 105495, https://doi.org/10.1016/j.engfailanal.2021.105495.
[4] V. Ribeiro, J. Correia, A. Mourão, G. Lesiuk, A. Gonçalves, A. De Jesus, F. Berto, Low-cycle fatigue modelling supported by strain energy density-based Huffman model considering the variability of dislocation density, Eng. Fail. Anal. 128 (2021) 105608, https://doi.org/10.1016/j.engfailanal.2021.105608.
[5] R. Branco, J.D. Costa, J.A. Martins Ferreira, C. Capela, F.V. Antunes, W. Macek, Multiaxial fatigue behaviour of maraging steel produced by selective laser melting, Mater. Des. 201 (2021) 109469, https://doi.org/10.1016/j.matdes.2021.109469.
[6] W. Macek, R. Branco, J.D. Costa, C. Pereira, Strain sequence effect on fatigue life and fracture surface topography of 7075–T651 aluminium alloy, Mech. Mater. 160 (2021) 103972, https://doi.org/10.1016/j.mechmat.2021.103972.
[7] W. Macek, R. Branco, J. Trembacz, J.D. Costa, J.A.M. Ferreira, C. Capela, Effect of multiaxial bending-torsion loading on fracture surface parameters in high-strength steels processed by conventional and additive manufacturing, Eng. Fail. Anal. 118 (2020) 104784, https://doi.org/10.1016/j.engfailanal.2020.104784.
[8] W. Macek, Fracture surface formation of notched 2017A–T4 aluminium alloy under bending fatigue, Int. J. Fract. 2021 (2021) 1–17, https://doi.org/10.1007/S10704-021-00579-Y.
[9] T. Kobayashi, D.A. Shockey, Fracture surface topography analysis (FRASTA)—Development, accomplishments, and future applications, Eng. Fract. Mech. 77 (12) (2010) 2370–2384.

[10] D. Sampath, R. Akid, R. Morana, Estimation of crack initiation stress and local fracture toughness of Ni-alloys 945X (UNS N09946) and 718 (UNS N07718) under hydrogen environment via fracture surface topography analysis, Eng. Fract. Mech. 191 (2018) 324–343, https://doi.org/10.1016/j.engfracmech.2017.12.010.
[11] D. Martelo, D. Sampath, A. Monici, R. Morana, R. Akid, Correlative analysis of digital imaging, acoustic emission, and fracture surface topography on hydrogen assisted cracking in Ni-alloy 625+, Eng. Fract. Mech. 221 (2019) 106678, https://doi.org/10.1016/j.engfracmech.2019.106678.
[12] R. Branco, J.D. Costa, L.P. Borrego, F. Berto, S.M.J. Razavi, W. Macek, Comparison of different one-parameter damage laws and local stress-strain approaches in multiaxial fatigue life assessment of notched components, Int. J. Fatigue. 151 (2021) 106405, https://doi.org/10.1016/j.ijfatigue.2021.106405.
[13] A. Carpinteri, G. Fortese, C. Ronchei, D. Scorza, A. Spagnoli, S. Vantadori, Fatigue life evaluation of metallic structures under multiaxial random loading, Int. J. Fatigue. 90 (2016) 191–199, https://doi.org/10.1016/j.ijfatigue.2016.05.007.
[14] Ł. Pejkowski, J. Seyda, Fatigue of four metallic materials under asynchronous loadings: Small cracks observation and fatigue life prediction, Int. J. Fatigue. 142 (2021) 105904, https://doi.org/10.1016/j.ijfatigue.2020.105904.
[15] Ł. Pejkowski, D. Skibicki, Stress-strain response and fatigue life of four metallic materials under asynchronous loadings: Experimental observations, Int. J. Fatigue. 128 (2019) 105202, https://doi.org/10.1016/j.ijfatigue.2019.105202.